ELSEVIER

Seminars in
NUCLEAR
MEDICINE

Small-Scale Dosimetry: Challenges and Future Directions

John C. Roeske, PhD,* Bulent Aydogan, PhD,† Manuel Bardies, PhD,‡ and John L. Humm, PhD§

The increased specificity of targeting agents has resulted in an interest in the use of radionuclides that emit particulate radiation: alpha particles, beta particles and Auger electrons. The potential advantage of these radionuclides is the ability to deliver therapeutic doses to individual tumor cells while minimizing the dose to the surrounding normal tissues. However, the dosimetry of these radionuclides is challenging because the dose must be characterized on a scale that is comparable to the range of these emissions, ie, millimeters for beta particles, micrometers for alpha particles, and nanometers for Auger electrons to. In this review, each class of particulate emitter is discussed along with the associated dosimetric techniques unique to calculating dose on these scales. The limitations of these approaches and the factors that hinder the clinical use of small-scale dosimetry are also discussed.
Semin Nucl Med 38:367-383

In recent years, there has been increasing interest in combining biologically specific targeting agents (ie, antibodies, peptides, etc.) with short-range particulate radiation emitters (alpha particles, beta particles, Auger electron emitters).[1-9] This therapeutic combination offers the potential of delivering lethal doses of radiation to individual tumor cells while minimizing the volume or normal tissue irradiated. Dosimetrically, these advances present a significant challenge. In the past, absorbed dose in nuclear medicine was often estimated at the organ level based on idealized models.[10-12] Calculation of absorbed dose on this scale has been sufficient for photon emitters used in imaging applications. However, for particulate emitters in therapeutic applications, the dose needs to be determined on a scale that is comparable with the range of emission. This scale is on the order of millimeters for beta particles, micrometers for alpha particles, and nanometers for Auger electrons. Although the formalism established by the Medical Internal Radiation Dose (MIRD) Committee may be adapted to these dimensions,[13,14] other factors also need to be considered. These factors include the effects of tissue heterogeneities,[15-17] stochastic variations in the amount of energy deposited in subcellular targets,[18-20] and the geometry of the target itself (ie, DNA).[21-24] In this review, we describe the calculational techniques used for short-range particulate radiation. Following a discussion of the MIRD method, each particulate radiation type is presented along with the specific calculational approaches that are unique to the emission. The limitations of these approaches along with the opportunities and future directions are discussed.

MIRD Method

In 1968, the MIRD Committee established the formalism for dose calculation from internally deposited radionuclides reducing the complex nature of the absorbed dose calculation into a simple mathematical form.[10] The MIRD schema provides methods for calculating the absorbed dose from the source-activity distribution and the physical properties of the radionuclide. This calculation is simply the conversion of activity in a source organ into the energy absorbed per unit mass in the target organ. In the MIRD schema, the mean absorbed dose, $\bar{D}$, within the k^{th} target from the i^{th} source is defined as:

$$\bar{D} = \tilde{A}_i \sum \Delta_j \frac{\phi_j\,(k \leftarrow i)}{m_k} \qquad (1)$$

where $\tilde{A}_i$ is the cumulated activity from the i^{th} source, Δ_j is the mean energy emitted per nuclear transition from the j^{th} transition, ϕ_j is the absorbed fraction, representing the fraction of

*Loyola University Medical Center, Maywood, IL.
†University of Chicago, Chicago, IL.
‡INSERM, Nantes, France.
§Memorial Sloan-Kettering Cancer Center, New York, NY.
Address reprint requests to John C. Roeske, PhD, Department of Radiation Oncology, Loyola University Medical Center, 2160 S First Ave, Maywood, IL 60153. E-mail: jroeske@lumc.edu

0001-2998/08/$-see front matter
doi:10.1053/j.semnuclmed.2008.05.003

energy emitted from the i^{th} source which is absorbed by the k^{th} target, and m_k is the mass of the target.[10] In this equation, Δ_j depends only on the decay properties of the radionuclide of interest and is given as the product of the number of particles (photons or electrons) of type j (n_j), and the mean energy per particle (E_j) of type j such that:

$$\Delta_j = K\, n_j E_j \quad (2)$$

where K is a proportionality constant with a value that depends on the units chosen for Δ_j and E_j. The absorbed fraction ϕ_j has values between 0 and 1 for penetrating radiations (photons) and is typically assigned to be equal to 1.0 for so-called "nonpenetrating" radiations (eg, alpha particles, Auger electrons, beta particles).

To further simplify the MIRD calculations, all physical data can be combined into single parameter known as the S value, which represents the mean dose deposited per unit cumulated activity,

$$S = \sum \Delta_j\, \phi_j(k \leftarrow i)/m_k. \quad (3)$$

Thus, the mean absorbed dose to the k^{th} organ, based on the MIRD schema, can be written as follows:

$$\bar{D} = \sum \tilde{A}_i S(k \leftarrow i). \quad (4)$$

Equation 4 can subsequently be rearranged as follows:

$$\bar{D} = A_0 \tau \sum S(k \leftarrow i) \quad (5)$$

where τ is the residence time which can be defined as the "average" or "effective" life of the initial activity (A_0) in the source organ. MIRD Pamphlet 11 characterized the S values for 117 radionuclides and many source/target organ pairs based on the MIRD anthropomorphic model.[11] Almost 20 years later, Stabin and Siegel published a compendium of nuclear medicine dose factors (an equivalent quantity to the S value as suggested by the authors) for 816 radionuclides.[25] This report used the most current decay data and phantoms for internal dose calculations.

Small-Scale Dosimetry

The development of the S value tables for a wide range of source/target organs and radionuclides have simplified internal dosimetry calculations. Moreover, the MIRD method is sufficiently general such that it can be applied to source/targets of any dimension (organs to subcellular regions).[13,14] However, the accuracy of these calculations is limited by the size of the source region that can be accurately quantified. Until the late 1970s, planar imaging was primarily used, and the MIRD method was only applied to organ-level dosimetry.[26-30] Suborgan dose calculations were made possible with positron emission tomography (PET) in the late 1970s and with single-photon emission computed tomography (SPECT) imaging in the early 1980s. These suborgan models included a multi-region heart[31] and kidney models.[12,32]

Quantification of nonuniform time-dependent activity (via PET or SPECT) with a resolution of 3 to 6 mm increased the accuracy of the MIRD method, thus allowing for voxel-based dosimetry. Dosimetry at this level is of interest in radioimmunotherapy, radioiodine therapy, and intratumoral radiopharmaceutical injections. MIRD Pamphlet 17 provides tabulated S values for 3 and 6 mm voxels from a nonuniform activity distribution for five of the most commonly used radionuclides.[33] This work has subsequently been expanded to voxel phantoms for internal dosimetry.[34] A comparison of internal radiation doses estimated by MIRD Pamphlet 17 and voxel techniques for a family of realistic phantoms was published in 2000.[35] These realistic phantoms were based on computed tomography (CT) images of humans. Because of the individual anatomical differences, some disagreements between these models and the MIRD model values were observed. Zankl and coworkers reported similar conclusions, including very large variations among voxel models for low-energy photon emitters.[34]

As more highly specific targeting strategies are developed that use short-range emissions (alphas, betas, Auger electrons), it is evident that the average dose at the organ or voxel level is less meaningful. For example, the mean organ or tumor dose alone does not correlate well with the biological effects observed with Auger electron emitters.[36] Within a group of cells, there is also considerable evidence that the dose individual cells receive may vary largely along with the associated biological response.[37] Thus, cellular and subcellular dosimetry has many applications in therapeutic studies where knowledge of the absorbed dose to individual cells and their nuclei is required. These applications include radiolabeled blood cells, ascites, isolated cells in an organ that preferentially incorporate a radiopharmaceutical, and cultured cells in the laboratory.

In 1997, the MIRD schema was extended to provide S values to calculate dose at the cellular level.[38] A simple cellular model was proposed consisting of two concentric homogenous spheres of unit density representing cell and cell nucleus. Figure 1 depicts the MIRD cell model showing the nucleus, cytoplasm and cell surface compartments. Typical cell diameters (R_C) and the corresponding cellular nucleus diameters (R_N) ranged from 6 to 20 μm and 4 to 18 μm, respectively. The activity was assumed to be uniformly distributed in one of the cellular compartments (ie, whole cell, cytoplasm, or nucleus). Cellular S values for emitters of mo-

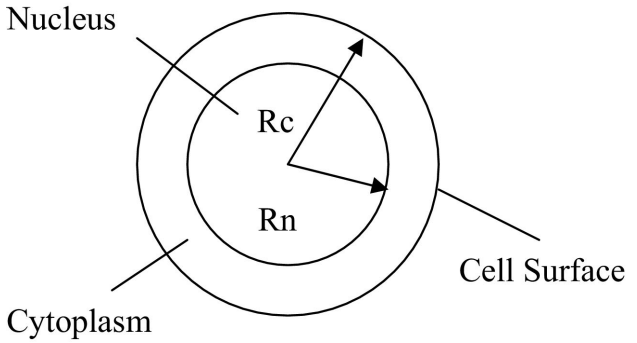

Figure 1 MIRD cell model (adapted from ref. 38) consisting of 2 concentric spheres representing the nucleus, cytoplasm and cell surface compartment modeled.

Table 1 S values in Gy/Bq-s for ^{90}Y Uniformly Distributed in the Cell for Various Diameters of Cell (R_C) and Nucleus (R_N) in Micrometers (μm)*

R_C	R_N	S(C←C)	S(C←Cs)	S(N←N)	S(N←Cy)	S(N←Cs)
7	3	1.23 E-04	8.19 E-05	6.79 E-04	1.14 E-05	5.63 E-05
8	7	9.41 E-05	6.25 E-05	1.23 E-04	6.32 E-05	5.19 E-05
8	6	9.41 E-05	6.25 E-05	1.68 E-04	6.78 E-05	4.78 E-05

*Adapted from the MIRD cellular S value monograph.[38]

noenergetic electrons, alpha particles, and many radionuclides were calculated and published for different source target pairs, including cell to cell (C←C), cell surface to cell (C←Cs), nucleus to nucleus (N←N), cytoplasm to nucleus (N←Cy), and cell surface to nucleus (N←Cs).

Several techniques have been used for calculating cellular S values, including both analytical and Monte Carlo (MC) methods. Hindorf and coworkers compared the mean absorbed doses calculated with the MC method[39] and published MIRD cellular S values[38] for monoenergetic electrons and reported agreement to within 4%. They attributed this small difference to the mass scaling of the MIRD S values to the cellular diameter used in their study to represent the B-lymphoma cell. Champion and coworkers have recently presented a MC code (CELLDOSE) and provided ^{131}I average dose estimates as well as dose distributions in spheres of various sizes down to 0.05 μm.[40] They reported S values that fell between those calculated using analytical methods[37,41] and previous MC calculations.[42]

Example

As a demonstration of how the MIRD schema is used to estimate cellular doses, consider the following calculation based on an example provided in the MIRD cellular S value monograph.[38] Radioimmunotherapy (RIT) is an established form of treatment for B-cell lymphoma. The ^{90}Y-labeled antibody, ibritumomab tiuxetan, is used in the treatment of follicular lymphoma. These antibodies bind to CD20—a surface molecule that is overexpressed on B-cell lymphocytes.[39] As a thought experiment, consider a sample of 10^6 B-cell lymphocytes labeled with 10 μCi (3.7×10^5 Bq) of ^{90}Y-antibody. The physical half life (T_p) of ^{90}Y is 64 hours, and we assume that it is eliminated from the lymphocytes with a biologic clearance half life (T_b) of 48 hours. Furthermore, we assume that 80% of the intracellular activity is localized in the nucleus. B-cell lymphocytes have an average diameter of 8 μm,[39] and we will assume that they have an average nucleus diameter of 6 μm. The goal is to calculate the average dose to the cell nuclei.

In this exercise, the initial cellular activity is simply the activity per cell assuming a uniform uptake in the cell sample. Below we calculate the required quantities to solve this problem:

$$A_{0,C} = \text{Initial cellular activity};$$
$$A_{0,C} = \frac{3.7 \times 10^5 \text{ Bq}}{10^6 \text{ cells}} = 0.37 \text{ Bq/cell} \quad (6)$$

T_{eff} = Effective half-life;

$$T_{eff} = \frac{T_p T_b}{T_p + T_b} = \frac{48 \times 64}{48 + 64}\text{h} \times 3600 \text{ s/h} = 9.87 \times 10^4 \text{ s} \quad (7)$$

$$\tilde{A}_c = \text{Cumulated activity};$$
$$\tilde{A}_C = A_{0,C} \times 1.44 \times T_{eff} = 5.26 \times 10^4 \text{ Bq-s} \quad (8)$$

From the Table 1, the mean absorbed dose to the cell nucleus per unit cumulated activity in the nucleus S(N←N) and cytoplasm S(N←Cy) are 1.68×10^{-4} Gy/Bq-s and 6.78×10^{-5} Gy/Bq-s, respectively.

The mean absorbed dose is given by Eq 5 and can be rewritten to accommodate activity in multiple compartments:

$$\bar{D} = \tilde{A}_C \times \{f_N \times S(N \leftarrow N) + f_{Cy} \times S(N \leftarrow Cy)\} \quad (9)$$

where f_N and f_{Cy} are the fraction of intracellular activity in the nucleus and cytoplasm, respectively. Thus, the mean absorbed dose is:

$$\bar{D} = 5.26 \times 10^4 \text{ Bq-s} \times \{(0.8 \times 1.68 \times 10^{-4}) + (0.2 \times 6.78 \times 10^{-5})\} \text{ Gy/Bq-s}$$
$$\bar{D} = 7.78 \text{ Gy} \quad (10)$$

Limitations

There are a number of limitations associated with the use of cellular S values as discussed in the monograph.[38] It should be noted that the cellular S values provided by Goddu and coworkers are mean self-absorbed doses and, hence, do not include the crossfire dose caused by activity on neighboring cells. Moreover, within a population of cells, the dose to an individual cell will depend on many factors, including its size and geometry, as well as the local activity distribution. Hence, the dose variation within a group of cells as a function of position may be required. To this end, many have questioned whether the mean absorbed dose to cell is a satisfactory measure to infer biological response in targeted therapy.[13,14,39,43,44]

Use of the average dose to an individual cell or at a particular point also assumes that equilibrium conditions are satisfied with respect to the number and type of particle entering and exiting a calculational volume. For low linear energy transfer (LET) radiation, a large number of decays is required to deposit a considerable dose, and hence this condition is generally satisfied.[45] However, this assumption may not be

valid when there is a very inhomogeneous cellular uptake or the cellular absorbed dose is low.[37] This assumption may also not be appropriate for alpha particles, where only a few cellular decays are required to inactivate a single cell.[46] In these cases, stochastic methods may be required. These and other dosimetric challenges will be discussed in the following sections.

Beta Particles

Beta emitters have been used for several decades within the context of targeted radiotherapy.[1] Even though ^{131}I is still the beta emitter most used within that context, ^{90}Y has also been widely used, for example, in RIT of non-Hodgkin lymphoma.[2] Several beta emitters have been investigated as potential candidates for targeted radiotherapy[47]; however, as stated in an early report by Rogus and Wessels,[48] dosimetric behavior is just one criterion among many governing the selection of a particular radionuclide.

Beta decay (negatron) decay occurs when the nucleus of atomic number A and mass number A is transformed into one with atomic number Z + 1 and mass number A and results in the emission of an electron.[49] The decay is symbolically represented by:

$$ {}^{A}_{Z}X \rightarrow {}^{A}_{Z+1}Y + \beta^{-} + \overline{\nu} \qquad (11) $$

where X and Y are the parent and daughter radionuclides, respectively, β^- is the electron released by the decay, and ν represents an antineutrino. Because the decay energy is shared between the beta particle and the antineutrino, the resultant beta particles have a spectrum of energies ranging from 0 to $E_{\beta max}$, where $E_{\beta max}$ is the energy of the transition. Typically, $E_{\beta max}$ is on the order of tenths to hundreds of keV, corresponding to a maximum electron range of several millimeters in water. This range brackets the scope of application of beta emitters: targeted radiotherapy relies on both vector specificity (to deliver the irradiation in situ) and short radiation range (to keep irradiation within the neighborhood of the emission point). ^{90}Y ($E_{\beta max}$ = 2.2 MeV) is the most energetic beta emitter considered for targeted radiotherapy, and its maximum range is ~1.1 cm in water, although 90% of the energy is deposited within the first few mm.[50]

Traditionally, the MIRD method treats beta emitters as nonpenetrating radiation with absorbed fraction $\phi = 1$. However, when the volume of interest is smaller than a few millimeters (ie, micrometastases), this assumption no longer holds true, and one has to calculate relevant absorbed fractions for the geometry and the radiation considered. This problem can be posed very simply. Consider a hypothetical point source in a uniform medium. If it is possible to define the energy transfer function (ie, the energy that is delivered at any distance from the point source) then it is also possible to calculate the energy delivered to a target volume from that point source. Based on the superposition principle, one can consider that any volume source is a superposition of many independent point sources. Hence the absorbed fraction (or the absorbed dose) can always be expressed in theory as a sextuple integral of the energy transfer function over the volumes of interest. However, defining and solving such integrals can be very difficult from a practical point of view.

Homogeneous Medium: Dose Point Kernel (DPK) Approaches

If the propagation medium can be assumed to be homogeneous (uniform density and composition), then the absorbed dose varies only as a function of the distance to the emission point. This important result is the basis of DPKs. DPKs provide the variation of the absorbed dose (or the absorbed fraction of energy) at a distance from an isotropic monoenergetic point source of electrons, in a homogeneous medium (usually water).[51,52] They can be used as input parameter for more complex geometries, following the superposition principle, as long as the medium is homogeneous.

The scaled point kernel $F(r/r_0, E_0)$ is defined by the following equation:

$$ F\left(\frac{r}{r_0}, E_0\right) = 4\pi \cdot \rho \cdot r^2 \cdot r_0 \cdot \Phi\left(r, E_0\right) \qquad (12) $$

where E_0 is the initial electron energy, ρ is the medium density, r_0 is the electron range under the continuously slowing down approximation (CSDA), and $\Phi(r,E_0)$ is the specific absorbed fraction at the distance r from the emission point. Scaling is obtained by dividing the distance r by the CSDA range, thus allowing for an easy comparison of DPKs of different energies. Scaled DPK have the characteristic that:

$$ 4\pi \cdot \rho \int_0^{\infty} r^2 \cdot \Phi\left(r, E_0\right) \cdot dr = 1. \qquad (13) $$

Most scaled DPKs are usually defined for r/r_0, varying between 0 and 1.2 to take into account the radiative emissions that deliver energy beyond the CSDA range.

DPKs proposed in the literature are obtained from measurements[53] or calculations,[49] sometimes using Monte-Carlo codes.[54,55] Monoenergetic DPKs can be integrated over the beta spectra to generate radionuclide DPKs.[56] Both monoenergetic and radionuclide DPKs have been used in dosimetric studies: radionuclides DPKs are usually used as an input for a geometric model whenever the study is considering a single radionuclide. However, whenever the goal is to compare the behavior of several radionuclides for a similar geometric problem, monoenergetic DPKs are used first to generate monoenergetic absorbed fraction tables, that are ultimately integrated over the relevant beta spectra.

Early measurements and mathematical descriptions of the beta DPK can be traced to the early work of Loevinger.[57] Electron fluence measurements were made for planar sources of a number of radionuclides as the beta particles were attenuated through sheets of polystyrene. By differentiating the dose as a function of position from a planar source and dividing by the distance, the kernel is obtained. Mathematically, the empirical function of Loevinger was described by an exponential term that represented the energy deposition due to unscattered and slightly scattered electrons, and a

linear-exponential term which represented the energy deposition by scattered radiation. While the Loevinger kernel provided an adequate description of the data over most of the beta particle range, it underestimated the dose near the point of emission.

Spencer[58] applied the method of moments and used the CSDA approximation to solve the transport equation for monoenergetic electrons. These results were used by Berger[51] and Cross and coworkers[59] to compile tables of point source energy deposition for a variety of beta emitters of clinical importance. However, Spencer's theory did not include the production of secondary electrons and their subsequent transport.

MC codes have also been used to estimate beta DPKs.[56,60] Prestwich and coworkers[56] applied this method to several radionuclides of interest in RIT. In comparison to previous results obtained by Berger, the DPK was lower near the origin, and higher near the maximum range. This difference is attributed to the fact that Berger's calculation did not include the effects of range straggling. Simpkin and Mackie[60] used the EGS4 MC program to estimate various dose point kernels in water. Their work showed minor disagreement with the results of Prestwich and coworkers because the latter used a code that improperly sampled the Landau spectrum. In their comparison with the data of Berger and Prestwich, Simpkin, and Mackie noted the DPK were generally in good agreement, although different assumptions and calculational methods were used.[60] Fujimori and coworkers compared three DPKs from the literature (Berger, Cross, and Prestwich) with their own, and found agreement was generally within a few percent for each of the data points.[61] Other MC codes been used more recently to generate DPKs, and again the general conclusion is that most current DPKs agree reasonably well.[62]

The complexity of dose calculations using DPKs varies with the source geometry. Whenever symmetries can be considered, analytic modeling is often possible.[63] As an illustration, consider the example of a very simple absorbed fraction calculation for unit density spheres (radius R_S) in an infinite homogeneous medium.[64] For the case of activity that is uniformly distributed at the surface of the sphere, the absorbed fraction in the sphere (radius = R_s) can be expressed by[64]:

$$\phi(R_S \leftarrow R_S) = \frac{1}{2r_0}\int_0^{\infty}\left(1-\frac{x}{2R_S}\right)\times F\left(\frac{x}{r_0},E_0\right)\times dx \qquad (14)$$

where $F(x/r_0,E_0)$ is the DPK at distance x from the emission point and r_0 is the CSDA range. Results for monoenergetic electrons are presented in Figure 2. For low-energy electrons, when the particle range is very small compared with R_S, the absorbed fraction tends toward 0.5 (semi-infinite medium condition). When the energy (and thus the particle range) increases, the absorbed fraction decreases since most of the energy is deposited outside the sphere. Another example is shown in Figure 3. For 100-μm radius spheres labeled on the surface, the variation of the absorbed dose per disintegration (the S factor according to the MIRD formalism, in Gy · Bq^{-1} · s^{-1}) in concentric spherical shells is represented for 3 beta emitting radionuclides (^{90}Y, ^{131}I, and ^{153}Sm). As demonstrated, significant dose gradients can be observed, particularly when the emitted energy decreases. The specific case of ^{153}Sm highlights the influence of monoenergetic electrons at short distances from the emission point.

For complex activity distributions (ie, when no obvious symmetry exists), as long as a homogeneous medium can be assumed it is still possible to use DPKs, but in this case convolution approaches are required. Mathematically, the dose at a point is expressed as a convolution integral:

$$D(\vec{r}) = \int f\left(\vec{r}-\vec{r'}\right)a\left(\vec{r'}\right)dr'^{3} \qquad (15)$$

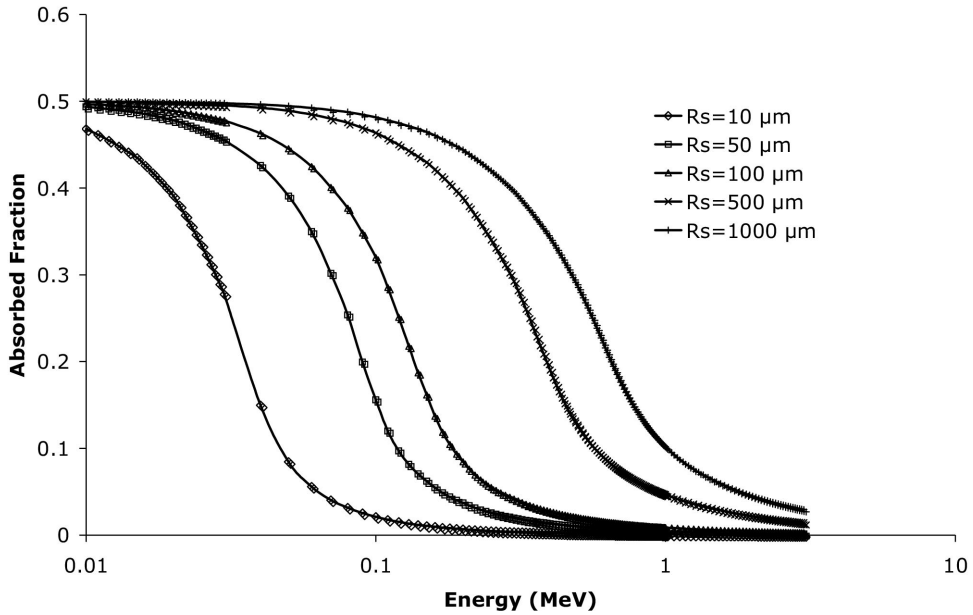

Figure 2 Absorbed fraction versus electron energy for unit density spheres (radius R_S) labeled on the surface.

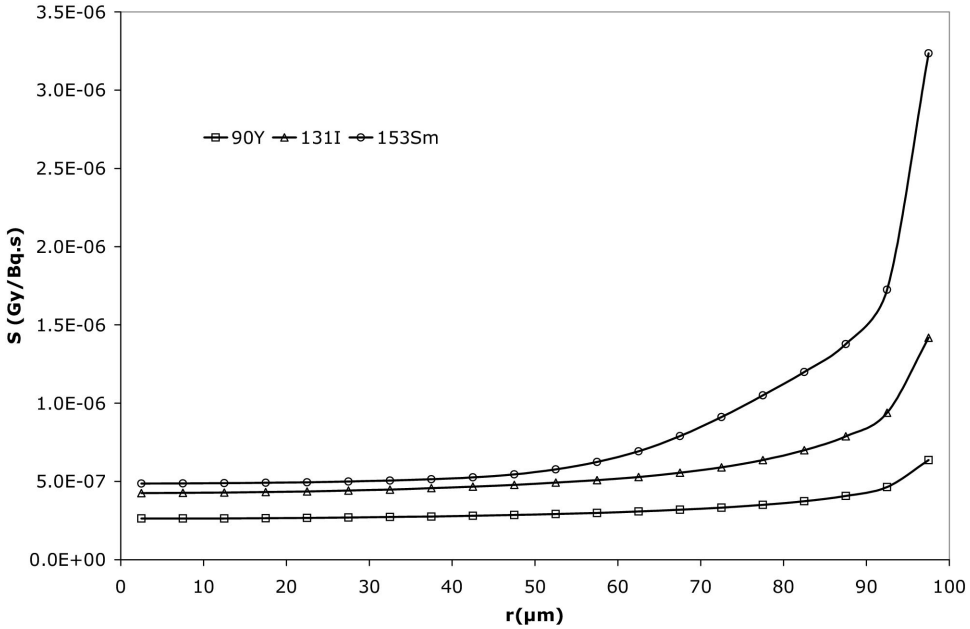

Figure 3 Variation of the absorbed dose inside unit density spheres labeled on the surface for 3 beta-emitting radionuclides.[64]

where $f(r - r')$ is the DPK, and $a(r')$ is the intensity of the source per unit volume. The evaluation of the convolution integral through analytical methods is difficult even for simple geometries. Therefore, numerical integration methods are often used. The convolution integration is replaced by a summation with discrete volume elements:

$$D(x, y, z) = \sum_{x,y,z} a(x', y', z') f(x - x', y - y', z - z') \Delta x' \Delta y' \Delta z' \quad (16)$$

where the primed variables represent the source position, and the unprimed variables represent the location of the calculation point in a Cartesian coordinate system. Note that for a full 3-dimensional calculation the computational time can become prohibitive.[65] Fast Fourier Transform[66] or Fast Hartley Transform[67] algorithms can be used to improve the speed of such calculations. In addition, MC approaches may also be used in homogeneous media for complex source/target geometries.[68]

Heterogeneous Media: Monte-Carlo Approaches

Whenever the surrounding medium is considered heterogeneous on the scale of the beta emission, DPK approaches are no longer valid and a full description of radiation emission, transport, and energy deposition is required. This is the domain of MC simulations. Two typical examples of the relevance of MC dosimetric modeling for beta emitters can be given: small-animal dosimetry and bone marrow dose modeling.

Small animals are often used within the context of targeted radiotherapy optimization. Dose calculations are usually performed from biopsy samples and activity counting (to assess the cumulated activity). Researchers often assume the beta particles are nonpenetrating. However, this assumption may not be valid for high-energy beta emitters and some small animal organs. To provide more accurate dosimetry, a simplified murine model was proposed in 1994 by Hui and coworkers.[69] More recently, several models were proposed using data collected from MicroCT or magnetic resonance imaging.[70-75] These models can be divided between mathematical (equation-based) and voxel-based.

The voxel-based mouse and rat models published by Stabin and coworkers[73] were obtained from MicroCT images, in which 10 to 15 organs were defined. Voxel dimensions were $0.2 \times 0.2 \times 0.2$ mm for the mouse and $0.3 \times 0.3 \times 0.5$ mm for the rat, whereas reconstruction was performed on a $256 \times 256 \times 256$ grid. A full 3D MC radiation transport and energy deposition process was implemented with the use of MCNP version 4C.[76] Absorbed fractions were calculated for 12 discrete initial electron and photon energies distributed in the source organs. A further integration of the absorbed fractions over the emission spectra led to dose conversion factors for ^{90}Y, ^{111}In, ^{131}I, and ^{188}Re. Bitar and coworkers compared the results obtained under the assumption of nonpenetrating radiation versus full MC absorbed dose calculation in the case of a small tumor xenograft, showing how important the difference could be for high energy beta emitters.[77]

Bone marrow dosimetry is another example of a highly heterogeneous medium at the microscopic scale, for which dosimetric approaches usually consider a full radiation transport modeling via MC. The absorbed fractions and S factors proposed by Cloutier and Watson[78] have been commonly used for many years. The model considered bone marrow

cavities as 400-μm spheres surrounded by 70-μm thick shells representing the bone walls. Spiers and coworkers at the University of Leeds first developed electron absorbed fractions for bone and marrow for an adult male subject. These results were used to calculate S factors in MIRD Pamphlet No. 11.[11] The ICRP[79] later proposed absorbed fractions derived partly from the work of Spiers. These calculations did not take into account the influence of backscattered radiation at the bone-soft tissue interface, which has been proven to be important.[15] MIRDOSE3 used a new dosimetric model proposed by Eckerman.[16,17] Bouchet and coworkers[80] used more recent information on regional bone and marrow mass, and calculated absorbed fractions using the EGS4 MC code.[81] A revised model has since been derived which resolves the differences between these 2 approaches.[82] The results were implemented in the OLINDA/EXM computer code.[83]

In summary, beta dosimetry is now at a mature age, with many approaches having been published that allow for consideration of a very wide range of geometry and radionuclides. DPK can be used when the propagating medium can be considered as homogeneous. For heterogeneous media, MC approaches are more appropriate. The usefulness of beta dosimetry essentially lies in preclinical validation of targeted radionuclide therapy and in the design of experiments to assess the relevance of a specific radionuclide within a given context.

Alpha Particles

In recent years, a number reports have characterized the use of alpha particle emitters in therapeutic applications.[3-6,84-86] Alpha particles consist of a helium nucleus with a charge of + 2, and are often the result of the decay of nuclei with an atomic number (Z) greater than 82.[49] Symbolically, the decay is expressed as:

$$ {}^{A}_{Z}X \rightarrow {}^{A-4}_{Z-2}Y + \alpha + \gamma \qquad (17) $$

where α represents the alpha particle and γ is a gamma emission that often accompanies the decay.[49] The alpha particles considered for therapy typically have an energy of 3 to 9 MeV. Their short range in tissue (40-90 μm) results in a significant amount of energy deposited near the point of emission. Moreover, the radiobiological advantages of alpha particles include their high LET and independence from dose rate and oxygen effects.[87]

The dosimetry of alpha-particle emitters is challenging because of the stochastic nature of energy deposited in small, subcellular targets.[88] The distribution of energy in these targets is often referred to as a compound Poisson process, a Poisson distribution in the number of events where the magnitude of each event varies. To illustrate this concept, consider cells in vitro that are irradiated by a uniform solution of alpha particle emitters (Fig. 4). We first define a "hit" as any alpha particle that intercepts the cell nucleus, regardless of the path length traversed through the structure.[88] Depending on the radionuclide concentration, some cells may receive no alpha particle hits. Other cells may receive one or more hits.

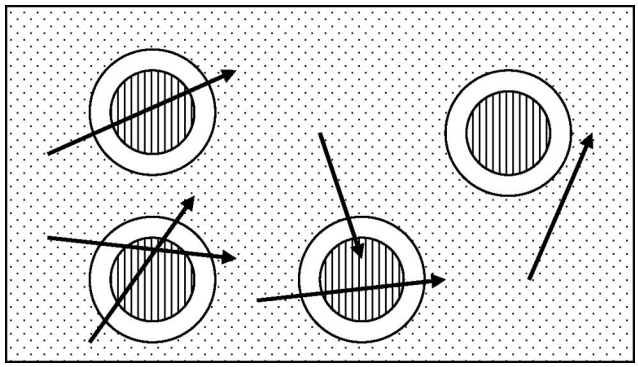

Figure 4 Schematic diagram illustrating microdosimetric concepts. The concentric circles represent individual cells and their nuclei. The lines with arrows are individual alpha particle emissions. Some cells receive multiple alpha particle hits, while others receive none at all. (Adapted from Roeske and Humm.[88])

Because the energy deposited is proportional to the track length of the alpha particle through the cell, those alpha particles that traverse the entire diameter will deposit a significant amount of energy compared with those that graze the surface. Thus, although each alpha particle would produce a single hit, the amount of energy deposited is quite different. Other effects that influence the energy deposited by alpha particles include the size and shape of the nucleus, variation in LET along an individual particle's path, and the point of alpha particle emission (within the cell versus. outside the cell, etc.).[88] On the basis of these factors, it is generally accepted that the dosimetric analysis of alpha particles requires microdosimetric methods.[89]

Microdosimetry is the study of the stochastic nature of energy deposition in small targets as a quantitative means of understanding the biophysical and biological interactions of radiation with matter. Originally proposed by Rossi,[90] microdosimetry was used to understand the stochastic nature of the energy deposited in matter by external ionizing radiation. Roesch[91] later adapted Rossi's theory to internally deposited radionuclides, such as Pu-239. Booz and Coppola[92] have applied this method for fast neutrons, Wilson and Paretzke[93] for protons, and Berger[94] for electrons. Fisher[18] applied microdosimetric methods to cells irradiated by ^{212}Bi for sources in various spatial configurations. Stinchcomb and Roeske[20] rigorously simplified Roesch's formulation for the case of antibodies labeled with short-lived alpha emitters.

The fundamental quantities in classical microdosimetry are specific energy (energy per unit mass) and lineal energy (energy per unit path length through the target).[89] These are often presented as a single event spectrum that represents the probability distribution for exactly one energy deposition event in the target. Alternatively, these quantities may be presented as a multiple hit spectrum that represents the distribution for N events. The multiple event spectrum (for N hits) may be determined by convolving the single event spectrum N-1 times.[90] Kellerer[95] developed a method to efficiently determine the multiple event spectrum through the use of Fourier transforms.

Microdosimetric spectra may be calculated with either analytical or Monte Carlo methods.[20,88] Analytical methods use a mathematical description of the path length through the target volume to determine the single-event spectrum. Convolution (via Fourier transforms) of the single-event spectrum is then used to calculate multi-event spectrum. MC methods involve a random sampling of the alpha particle emission, and then trace the alpha particle's path through the medium. Depending on the level of sophistication, these codes may simulate each interaction along the particle's path,[96] or they may make some assumptions about the alpha particle's path (such as being a straight line), and determine the energy deposited in the target from range-energy tables.[97] In general, Monte Carlo codes provide greater flexibility than analytical methods, and can simulate a wide range of complex geometries.

A Simple Monte Carlo Code

Roeske and Hoggarth[97] describe a simple alpha particle MC code that was implemented using a commercial spreadsheet with a random number generator. The components of this approach are described here to illustrate how Monte Carlo may be used to generate single-event spectra. As with any algorithm, a series of assumptions are made. Similar to the MIRD cellular model, the cell and nucleus are assumed to be spherical and concentric. The user has the options of generating spectra for any of four source compartments: nucleus, cytoplasm, cell surface, and outside the cell. On the basis of the chosen compartment, individual alpha particle particles are assigned a random point of emission. Note that because the cell and nucleus are both spherical, this point of emission only needs to be expressed as a radial coordinate.

Next, a random emission direction is chosen, and the path of the alpha particle is tracked. In this study, the alpha particles are assumed to travel in straight lines. Polig[89] demonstrated that such an approximation is valid for alpha particles with energies less than 10 MeV. In addition, because the nucleus is considered to be the target (diameter >1 μm), the width of the alpha particle track can be ignored as it is significantly smaller ($\sim$100 nm). Using these assumptions, the parameteric equations of a straight line can be used to determine whether the alpha particle intersects the nucleus.[98] By solving a quadratic equation, the entrance and exit points for the alpha particle's intersection with the nucleus can be determined.[97] Note that when the alpha particle emission occurs in the nucleus, only the distance to where the alpha particle exits the nucleus is required.

The energy deposited is determined by subtracting the energy of the particle as it exits the nucleus from the energy that it enters the nucleus.[88] In cases where the alpha particle stops inside the nucleus, the former is set to zero.[88] The energy deposited is determined from alpha particle range-energy tables. These data for a variety of media can obtained from the literature.[99-101] The CSDA approximation is used in this approach.[102] Using the same source-target geometry as Humm,[19] Stinchcomb and Roeske[20] compared specific energy distributions using different range-energy tables. Specifically, they compared Janni's range-energy tables[103] for protons (appropriately scaled for alpha particles) to Walsh's data.[104] They observed differences in the average specific energies on the order of 1% to 7%. Roeske and Hoggarth[97] subsequently used data from ICRU Report 49 for water (ICRU 1993) in their simulations and observed good agreement with Stinchcomb and Roeske.[105] In practical situations, it is expected that the uncertainty in the activity distribution will be much larger than that of the range-energy data used in the simulation.[88]

The energy deposited (E) can subsequently be used to calculate the specific energy (z) through the following equation:

$$z = E/m \tag{18}$$

where m is the mass of the cell nucleus. The mass of the nucleus can be estimated as the product of the volume and the density (in this case assumed to be 1 g/cm^3). For each alpha-particle emission in the simulation, the specific energy is computed. A histogram of these specific energies is subsequently calculated to determine the single-event spectrum. Example single-event spectra for are shown in Figure 5.

This algorithm can also be extended to determine the multi-event-specific energy spectrum.[88] In this case, an explicit concentration (or number) of alpha particle emissions is simulated, and all are evaluated to determine if they intersect the cell nucleus. Of those that intersect the nucleus, the energy deposited and the total specific energy is calculated for this individual simulation. This scenario represents one possible outcome.[88] To sample all possible outcomes, the simulation is repeated many times. A histogram of these individual results is the multi-event distribution.[19,20,88] As described previously, single-event spectra can be convolved with itself multiple times to determine the multi-event spectrum. Such an analysis requires knowledge of the average number of hits for a particular source configuration, as well as the distribution of these. Often Poisson statistics are used. Stinchcomb and Roeske[20] demonstrated that both methods produce the same multi-event spectra within the uncertainty of the calculation itself.

Microdosimetric Applications

One application of microdosimetry has been in the theoretical and experimental analysis of cell survival. For a single–event spectrum the surviving fraction is given by eq 19[20,88]:

$$S(\bar{z}) = \exp[-\langle n\rangle\{1 - T_1(z_o)\}] \tag{19}$$

where $<n>$ is the average number of hits to the cell nucleus, and $T_1(z_o)$ is the Laplace transform of the single-event spectrum. For a multi-event spectrum, the relationship is given by eq 20[20,106,107]:

$$S(\bar{z}) = \int_0^\infty f(z)e^{-z/z_o}dz \tag{20}$$

where $f(z)$ represents the fraction of cells receiving specific energies between z and $z + dz$. In both cases, z_o is the specific

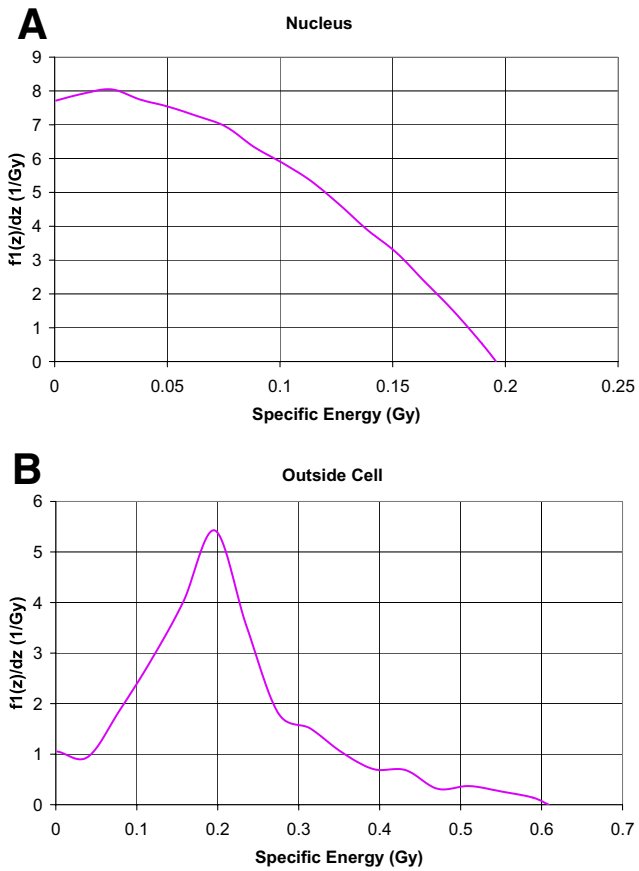

Figure 5 Single-event spectra for an 8.78 MeV alpha particle emitted (A) in the cell nucleus and (B) outside the cell. The nucleus and cell diameters are 10 and 14 μm, respectively. (Color version of figure is available online.)

energy deposited within an individual cell that reduces the average cell survival to 1/e, and $\exp(-z/z_o)$ is the fraction of cells that survive. The use of an exponential survival model assumes that there are no bystander effects and that intratrack interactions are dominant relative to intertrack interactions. Note that z_o is not equal to D_o, which is determined from the slope of the cell survival curve. Rather it is a more fundamental quantity as D_o has folded into it not only the effects of the radiation, but also the effects of the source-target geometry.

Humm[19] combined the multi-event specific energy distribution with a model for cell survival to analyze the impact of stochastic energy deposition on the expected surviving fraction of a group of cells. Two geometries were considered: cells located outside of a capillary and cells located within a tumor consisting of a uniform distribution of ^{211}At. The results of this analysis demonstrated that although the mean dose was similar for both geometries, there was a significant variation in the expected cell survival due to the differences in the specific energy spectra. In particular, the fraction of cells without alpha-particle hits increased with distance from the capillary (due to the short range of the alpha particles) resulting in a bi-exponential cell survival curve. Others have extended these theoretical studies to different cell geometries and source configurations.[107-112] Among the results of these analyses is the conclusion that the most important factor affecting the cell survival is the source configuration with highly nonuniform source distributions producing survival curves that deviate from the standard mono-exponential curve.

Others have used the aforementioned approach to analyze cell survival to determine the inherent cell survival, z_o. Stinchcomb and Roeske[113] applied the previously developed methods of predicting cell survival to the analysis of experimentally produced cell survival curves. By calculating the specific energy distribution and knowing the resultant cell survival for irradiation condition, they determined z_o by using iterative methods. Larsen and coworkers[112] used a microdosimetric approach to determine the inherent cell sensitivity of human glioma and melanoma cell lines. This analysis revealed that the sensitivity of individual cells was much greater than would be expected using a nonstochastic dose analysis. Charlton[110] made refinements to the Larsen[112] model by incorporating the effects of finite cluster sizes, and illustrated the importance of accurately modeling cell geometry and its effect in interpreting cell survival studies. Aurlien and coworkers[111] compared the biological effects of ^{211}At radioimmunoconjugates to external gamma rays for osteosarcoma cells.

An additional level of complexity above single cells in suspension involves the microdosimetric analysis of multicellular spheroids which mimic micrometastatic clusters. Kennel and coworkers[114] considered cell survival after the irradiation of multicellular spheroids with an alpha-particle emitting radiolabeled antibody. Charlton[115] calculated microdosimetric spectra for multicellular spheroids and simulated their subsequent survival. In both studies, the specific energy distribution is a function of depth inside the spheroid. Thus, a single specific energy distribution is not representative of that through the entire tumor. Combining specific energy distributions with a model of cell survival may provide an overall measure of the therapeutic effectiveness, however, these cell survival models do not take into account second order processes such as bystander effects. These processes are more difficult to simulate and may play a significant role for these types of geometries. The ongoing refinement of these cell survival models is currently an area of active research.[116]

Another area for which microdosimetric calculations are important is bone marrow as it is often the dose-limiting organ in RIT. As discussed previously in this report, bone marrow dosimetry is difficult because of the complex geometry as well as the presence of tissue inhomogeneities. Thus, idealized models, as have been used in the previous studies, must be replaced by more realistic geometries. Studies estimating microdosimetric spectra for bone marrow have focused largely on using histological samples obtained from humans or animals. Bone marrow microdosimetry has been used for radiation protection purposes[117-120] and for limited clinical studies.

Akabani and Zaltusky[121] measured chord length distributions through histological samples of beagle bone marrow. Using a MC program, they calculated specific energy spectra and combined these with a model of cell survival. Their anal-

ysis demonstrated that activity distributed on the cell surface resulted in higher levels of cell kill than activity in the extracellular fluid. Charlton and coworkers[119] calculated microdosimetric spectra and subsequent cell survival based on geometries from human marrow samples for two different radionuclides – ^{149}Tb and ^{211}At. These simulations indicated that for targeted decays, ^{149}Tb was 5 times more effective than ^{211}At when compared on a hit-by-hit basis. This enhancement was a consequence of the lower energy of ^{149}Tb, resulting in a higher LET of the incident alpha particles. Recently, small-scale imaging techniques (microCT and magnetic resonance) have been used to obtain a more detailed geometry of the skeletal microstructure.[122,123] As these imaging data are incorporated into microdosimetric calculations, further refinements of these results are expected.

Utteridge and coworkers[124] considered the risk of developing secondary malignancies (ie, leukemia) from alpha particles. On the basis of modeling, they determined that short-ranged alpha particles had a lower risk of causing a secondary malignancy relative to long-ranged alpha particles. Fakir[125] recently combined a generalized state-vector model of carcinogenesis with single-track alpha particle depositions.

To summarize, the microdosimetry of alpha particles is well characterized. A number of theoretical and in vitro studies have been performed over the years. In all of these studies, microdosimetric analyses have provided additional insight into the underlying radiobiology that would not be afforded by conventional dose estimates alone.

Auger Electrons

There are many radionuclides that decay by a process known as electron capture. Electron capture is a beta decay process that competes with positron emission. For nuclei, which are unstable because of an excess of positive charge, this positive charge can be reduced by the transformation of a proton to a neutron with the emission of a positron, or alternatively by nuclear capture of an orbital electron.[49]

$$p^+ + e^- \rightarrow n + \nu_e \qquad (21)$$

Whereas there are no emissions directly from the nucleus, the residual inner atomic shell vacancy is rapidly filled by inner shell electron transitions that progressively move the vacancy to the outermost atomic orbital. Each electron transition may result in the emission of a characteristic X-rays or an Auger electron (Fig. 6). While the textbook handling of this subject largely emphasizes the emission of characteristic X-rays, the nonradiative transitions involving the ejection of an Auger electron is more common, especially for low Z atoms. The energy of Auger electrons correspond to the difference between the energy gained by the electron orbital transition minus the binding energy of the orbital from which the electron is ejected.

Another radioactive decay process culminating in similar consequences to electron capture is internal conversion, because it too results in the production of an inner shell electron vacancy. Internal conversion, as its name implies is an alternative way for the nucleus to return to the ground state, without the emission of a gamma ray, but rather the ejection of an electron with an energy which is equal to the residual nuclear excitation energy minus the binding energy of the inner shell orbiting electron. Both electron capture and internal conversion can affect all atomic orbital electrons. However, in both processes, interaction with the K-shell is far more probable (if allowed energetically), because the inner shell electron orbitals overlap with the nucleus.

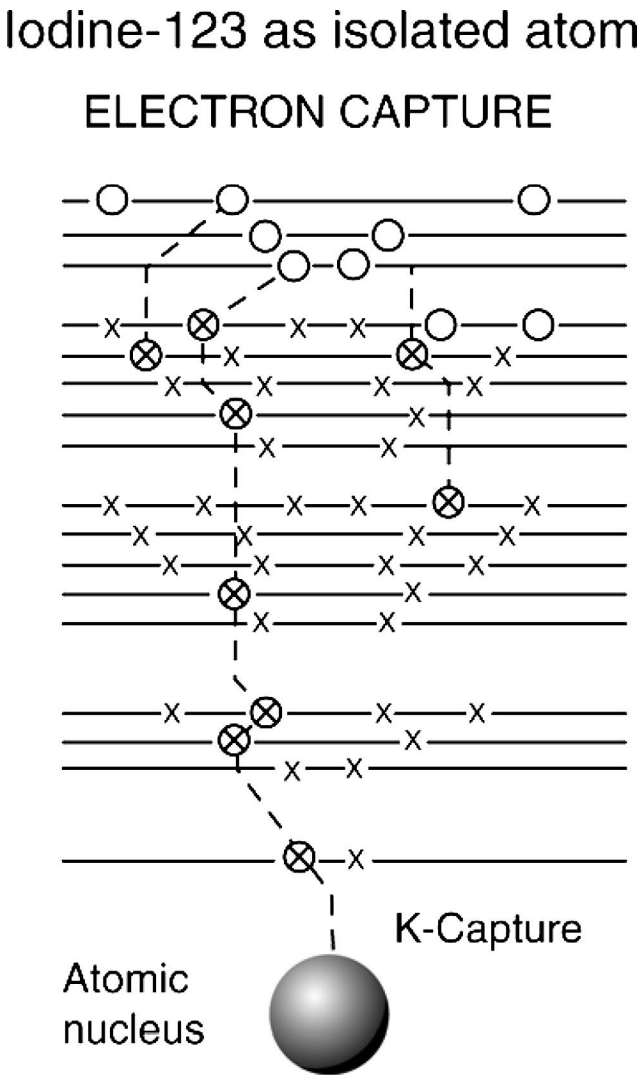

Figure 6 Schematic diagram illustrating an ^{123}I atom undergoing electron capture. In this diagram, the crosses represent an electron in its shell. Vacancies are denoted by empty circles while circles with crosses are filled vacancies. Each transition moves a vacancy to a higher orbital until all of vacancies occupy the outermost shells. (Reprinted with permission of Taylor & Francis Group LLC from Roeske and Humm.[88])

The filling of this inner shell vacancy results in the emission of a series of fluorescent but predominantly nonradiative Auger transitions. The rules which govern the filling inner shell vacancies is the fluorescence yield, which defines the partition between radiative (radiograph) and nonradiative (Auger) transitions (of significance only for K-shell transi-

tions), and the numerous competing nonradiative transition probabilities between electron orbitals and suborbitals. Once the vacancy has reached the L and higher shells, it is common for transitions between shells to result in both electrons being ejected from the same or adjacent suborbits, eg, $L_1M_1M_1$ and $L_1M_1M_2$. When this happens, the event is referred to as a Coster-Kronig transition.

MC methods have been used to calculate the stochastics of the atomic de-excitation pathway through an atom, each one resulting in an individual Auger and Coster-Kronig electron spectra. The first MC code to calculate Auger electron spectra was developed by Charlton and Booz,[126] who used a normalized database of inner shell transition probabilities to each orbital vacancy from higher shells and subshells. The energy of the emitted electrons was calculated using the $Z/(Z + 1)$ approximation[127] that is based on a weighted ratio of the binding energies between the parent and daughter atoms. In this implementation, the first random number is used to select an inner shell vacancy (from electron capture or internal conversion) weighted in accordance with the probabilities of an event occurring in the K, L, and higher shells.

An Auger electron transition consists of an electron falling from a higher orbital to fill the inner shell vacancy, thereby shifting the location of the vacancy to an orbital of lesser binding energy. The energy gained by this electron transition is used to liberate an electron (the Auger electron) from a higher orbital. Thus, an Auger transition results in the filling of one vacancy, concomitant with the creation of 2 new vacancies. MC simulations of this process proceed by selecting a transition to the deepest atomic vacancy until all vacancies have reached the outermost electron shells. The binding energies of the electron orbitals change when there are multiple vacancies and these are not realistically taken into account by the $Z/(Z + 1)$ approximation, which is only strictly valid for the first Auger transition. Pomplun and coworkers[128] solved this electron energy estimation by using an elaborate precalculated look-up table for the most frequent multi-electron vacancy configurations using the Dirac-Fock computer codes developed by Desclaux.[129]

Once these vacancies reach the outermost orbitals of the atom, they represent a positive charge of magnitude equal to the number of ejected electrons. Radiochemists have long shown that when an electron capture decaying atom is attached to a molecule, such as methyl ^{125}I, this rapid charge build-up results in a so called "Coulomb explosion" in which the molecule becomes significantly fragmented. Studies of electron capture and internal conversion atoms in the gaseous state have allowed the charge spectra to be measured directly.[130]

A substantial number of electron capture decaying nuclides result in an excited daughter nucleus and subsequent internal conversion. For example ^{125}I undergoes electron capture followed by a 0.93 probability of internal conversion and 0.07 probability of gamma ray emission. ^{123}I undergoes electron capture followed by a 0.16 probability of internal conversion and 0.84 probability of gamma emission. For these 2 radionuclides, 2 Auger electron cascades ensue for a significant fraction of the decays. Whereas excited nuclei are typically short lived (in the case of the excited ^{125}Te and ^{123}Te nuclei of the order of a nanosecond), there are a few important radionuclides which exist in metastable excited states for times long enough to make them useful in medical imaging, the best known of which is ^{99m}Tc. These decay processes are isometric transitions, in which the parent and daughter atom are identical, the only emissions being gamma or internal conversion electrons (with Auger cascade).

It was initially believed that this fluence of low-energy Auger electrons would result in inconsequential radiation doses. For this reason, radionuclides which decay by electron capture or internal conversion were deemed most suitable for use in tracers for nuclear medicine applications, eg, ^{67}Ga, ^{99m}Tc, ^{123}I, and ^{201}Tl. Fortunately, the safety record of nuclear medicine procedures underscores that radiopharmaceuticals using electron capture and internal conversion decaying radionuclides do not produce unexpected radiobiological effects or elevated carcinogenic incidence, as anticipated by a very low electron emissions and the radiation dose they deposit. However, when these radionuclides are appended to molecules that directly target radiation sensitive structures within the cell such as the DNA, radiobiological damage can become manifest commensurate with that of high LET alpha particles. The first demonstration of the high radiotoxicity of Auger electron emitters were the studies with ^{125}I-labeled thymidine precursor iododeoxyuridine (^{125}IUdR) by Ertl and coworkers,[131] Burki and coworkers[132] and Hofer and coworkers.[133] The steepness of the radiation survival curves resulting from ^{125}I relative to tritiated thymidine, whether expressed per decay or per unit cellular dose, led investigators to realize something significant about the energy deposition from Auger electron emitters.

Studies modeling the detailed atomic transitions from electron capture and internal conversion decaying nuclides, combined with track structure simulations of the local energy deposition showed the ability of iodine isotopes such as ^{125}I and ^{123}I to deposit a dense cloud of energy close to the decay site, typically in the range of nanometers, that can exceed the local ionization density within the core of an alpha particle track.[21,126] The high-energy deposition local to the site of decay allows these nuclides to probe the cell for radiation sensitive targets, and has generated the most decisive evidence that the nuclear DNA is the most radiosensitive element for cell death. In fact comparative cell survival studies in which ^{125}I is incorporated into mitochondrial DNA[134] or the cell membrane[135] require orders of magnitude more decays to achieve the same levels of cell inactivation. Radiosensitivity is exquisitely sensitive to location as has been shown from studies in which ^{125}I was intercalated between the major and minor groove of the DNA rather than directly incorporated via a thymidine analog.[136] Studies with ^{125}I-IUdR also provided key data to show that high LET-like induced double-strand breaks are correlated with reproductive survival.

More recent studies have investigated the effectiveness of ^{125}IUdR decays when incorporated into the DNA during early versus late S-phase in Chinese hamster V79 to 379A cells. A greater yield of DNA double-strand break production was observed in late S phase in the presence of 10% dimethyl

sulfoxide compared with early S phase. Moreover, a nonrandom fragment distribution implied an effect of chromatin organization on the damage manifestation. This disparity in double strand break yields were not observed in similar experiments performed on naked genomic DNA.[24]

Although the largest body of work has been studies investigating the radiobiology of Auger electrons has been with ^{125}I,[8,137] numerous studies have been conducted with other important Auger electron emitters. First, there are researchers investigating other electron capture and internal conversion decaying halogens, such as ^{77}Br and ^{80m}Br and their effectiveness when incorporated into the DNA via the thymidine precursor bromodeoxyuridine.[7,138] An intercomparison of the radiotoxicity of different Auger electron emitters show that the magnitude of the radiobiological effectiveness depends on the branching ratio for the electron capture and/or internal conversion events per decay, eg, ^{125}I versus ^{123}I[139] and the size the Auger electron cascade which depends on the atomic number Z, eg, ^{125}I versus ^{77}Br.[138]

An example of a large electron capture-decaying radionuclide used routinely in nuclear cardiology is ^{201}Tl. In vitro studies investigating the radiotoxicity of intracellular ^{201}Tl have been performed by Kassis and coworkers.[140] Thallium-201 selectively accumulates in cells via the potassium/sodium pump, resulting in enhanced radiotoxicity consistent with the short-range nature of Auger electrons but not equivalent to the high LET-like effects seen with radio-halogens selectively incorporated within the DNA. Human investigation of the uptake of ^{201}Tl showed some selected accumulation in the testes.[141] Measurements of testicular uptake and clearance of ^{201}Tl in humans, by gamma camera imaging, showed rapid uptake to approximately 0.4% of the injected dose with a long biological retention (clearance half-time of 280 hours). Average absorbed dose to the testes was reported to be 3.5×10^{-4} Gy/MBq (1.3 rad/mCi) increasing to an equivalent dose of 9.5×10^{-4} Sv/MBq (3.5 rem/mCi), when accounting for the measured radiobiological effectiveness resulting from intracellular accumulation of ^{201}Tl. Other smaller atoms are expected to result in lesser radiobiological effectiveness, unless specifically incorporated into the cellular genome or other sensitive cell for cellular inactivation.

The most widely used nuclear medicine tracer is ^{99m}Tc. This nuclide emits a gamma ray (140 keV), but also low-energy Auger and conversion electrons. MC computer codes to simulate the track structure resulting from these emitted electrons (4 on average per Auger cascade) by Pomplun and coworkers[142] revealed a nearly identical spectrum of primary DNA strand breaks for ^{99m}Tc and carbon K-shell 247 eV ultrasoft X-rays. On this basis, Pomplun and colleagues recommended a radiation weighting factor of 1.2 for ^{99m}Tc decays. Experimental studies to determine the radiotoxicity of 3 ^{99m}Tc-labeled compounds (pertechnetate [^{99m}TcO4−], pyrophosphate [^{99m}Tc-PYP], and hydroxyethylene diphosphate [^{99m}Tc-HDP]), using spermatogenesis in mouse testis as the experimental model, have been performed by Narra and coworkers.[143] The mean lethal doses at 37% survival were reported as 0.70, 0.84, and 0.59 Gy for ^{99m}TcO4-, ^{99m}Tc-PYP, and ^{99m}Tc-HDP, respectively. These results yielded RBE values for these compounds of 0.94, 0.79, and 1.1, respectively. More importantly, the radiotoxicity of internal emitters, especially Auger electron emitters, is extremely sensitive to the carrier molecule and its relative distribution at the cellular and subcellular level. These data show that the Auger electrons emitted by commonly used ^{99m}Tc radiopharmaceuticals do not selectively transport the radionuclide into or in close proximity of the cellular genome and that the dose modification factor of 1.2 recently proposed by Pomplun and coworkers,[142] is a conservative estimate based on an intranuclear concentration.

As new radiopharmaceuticals are developed, new radionuclides may be considered. To perform dosimetry calculations for these nuclides, it is first necessary to obtain the Auger and Coster-Kronig electron spectra. A number of such spectra for this purpose have been provided in the AAPM task group report prepared by Howell,[144] following the method developed by Charlton and Booz.[122] An example for ^{123}I is shown in Figure 7. Methods to perform dosimetric calculations from these spectra are provided by Humm and coworkers.[145] Auger spectra corresponding to radionuclide of interest are used to calculate the local radiation energy deposition from electron capture and internal conversion decaying radionuclides. The highly local and stochastic nature of Auger electron energy deposition has resulted in the preferred use of specific energy, z, or energy deposition, ε, spectra rather than the macroscopic measure of absorbed dose. With the use of the Auger electron spectra resulting from individual decays, the electron tracks are simulated through liquid water (or unit density water vapor), a medium for which the electron interaction cross sections are well known down to an energy of 10 eV. The electrons travel a distance determined by a random number generator, weighted in accordance with their mean free path corresponding to the electron energy. The coordinates of each electron interaction within water is recorded, together with the local energy deposited, and the directional cosines of the primary electron plus any delta rays

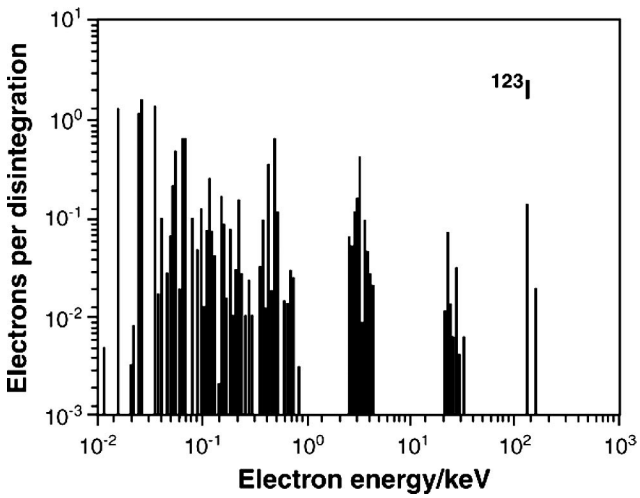

Figure 7 The average electron energy spectrum from ^{123}I based on the simulation of 10,000 decays. (Reprinted with permission of Taylor & Francis Group LLC from Roeske and Humm.[88])

emanating from that interaction point. These recorded energy deposition events can be summed within concentric spheres around the decay site to score energy deposition (or specific energy) as a function of sphere size. Alternatively, the coordinates of the energy deposits may be superimposed on a detailed geometric model defining the spatial location of each chemical atom in the DNA. Note that currently there is insufficient information to directly model the electron interactions within the DNA-histone moiety, and therefore such models consist of numerous simplifications. However, these models are extremely useful and provide a wealth of information on the stochastics of microscopic energy transport and energy deposition.

Many dosimetric calculations with Auger electron emitting radionuclides do not require such advanced calculations but can reliably use the cellular S factors. The necessity of such detailed modeling only becomes important for cases in which the radiopharmaceutical associates with the cellular genome either by chance or by design such as in the field of Auger electron targeted therapy. Very simple geometric models of the DNA double helix are used, consisting of 3 block segments: a central cylindrical core, to represent the nucleotide pairs, surrounded by a C on each side interlocking to tightly enclose the central nucleotide cylinder, each C representing an individual DNA strand. The Cs are rotated every 3.6 nm by 10° so as to model the helical rotation.[22] This model was used to calculate the local energy deposition at the subnanometer level initially for ^{125}I and, later, other radionuclides.[146] By matching the stochastic energy deposits within a geometric representation of the double stranded DNA and comparing with the resulting strand breakage relative to the site of ^{125}I incorporation measured with DNA sequencing gels by Martin and Haseltine,[147] it was possible to estimate a threshold energy for probable strand break damage to be 17.5 eV. More recent analyzes based on greater resolution and precision DNA strand break damage, which includes the influence of the radical scavenger dimethyl sulfoxide have been conducted by Nikjoo and coworkers.[23] This model includes the creation of water radical production and diffusion of the radiochemical species relative to the target strands. There are further advances in the computer models used to simulate the DNA, which now includes a more exact chemical representation of the DNA, and which can be used to determine the atom in closest proximity of each energy deposition event. [9,148,149]

Radionuclides that emit Auger electrons are in widespread clinical use in nuclear medicine. Absorbed dose calculations for such radionuclides in man are based on tabulated S-factor calculations, based on organ biodistribution data ascertained from gamma camera (or PET) images. The utility of these dosimetric estimates relies on the nonselective intranuclear incorporation of these agents.[150] If a fraction of the radionuclide carrier becomes intracellular, intranuclear and most important DNA-associated, then the biologically effective dose increases. A method to calculate equivalent dose for Auger electron emitting radionuclides given a nonuniform cellular distribution of organ uptake is given by Goddu and coworkers.[151]

Of final importance are the mutagenic effects of ^{125}I decays when incorporated into the DNA via ^{125}IUdR compared against tritiated thymidine. Liber and coworkers[152] used the mutant 6-thioguanine resistance in human lymphoblastic cells and found at low doses a 20-fold greater yield of mutations/decay of 1×10^{-6} for ^{125}IUdR versus 2×10^{-8} for tritiated thymidine.

In summarizing the experience of those radiobiologists who have focused on the effects of Auger electron emitting radionuclides, a number of conclusions may be drawn. The radiobiological effectiveness of Auger electron-emitting radionuclides is highly dependent on the carrier molecule, which will determine its extra/intracellular distribution. The survival curves produced by Auger electron emitting radionuclides most commonly resembles the shouldered survival curve exhibited by other low LET radiations, eg, radiograph and beta particles. However, carrier molecules that deliver an Auger electron emitting radionuclide into close proximity of the nuclear DNA may result in significantly increased radiobiological effectiveness that resembles an alpha particle (linear) survival curve response. This enhanced radiotoxicity is explained by a combination of track structure calculations revealing the cluster of dense ionizations around the atomic decay site resulting from the Auger cascade and the positive charge build up and ensuing Coulumb explosion leading to molecular fragmentation. Methods to determine an equivalent dose for Auger electron emitting radionuclides are available if the microdistribution, and apportionment of intranuclear and DNA associated decays of the radiopharmaceutical can be obtained.

Summary

The principles of small-scale dosimetry for alpha particle, beta particle and Auger electron emitting radionuclides have been in existence for several years. These calculational techniques have been applied to a number of studies – theoretical, in vitro and to a lesser amount, in vivo. Two general calculational approaches have been used. Analytical methods are based on equations that parameterize the energy deposited from individual source emissions.[20,51,52,88] These calculations are fast and can take advantage of computationally efficient computer algorithms.[66,67] MC techniques simulate individual particles and their interactions through the medium.[56,60,68,76,96,97,117,119,128] This class of calculation is best suited for complex source/target geometries and in cases where tissue inhomogeneities exist.[80-83,119,123] To a great extent, both approaches have been shown to yield comparable results for many situations.

Unfortunately, small-scale dosimetry has had limited application in clinical practice. Accurate and complete small-scale dosimetry requires knowledge of the source distribution as a function of time on the cellular/subcellular scale. In the clinic, activity determination is mainly based on quantitative scintigraphic imaging, ie, with a spatial resolution on the order of mm. At this scale, these emissions are typically considered as nonpenetrating radiations, even when voxel-based activity determination is considered. Assessment of the

geometric target is even more difficult as the target can range from single cells in suspension (ie, ascites, blood-borne diseases) to small metastatic clusters to potentially macroscopic tumor masses. Clearly, the scale of target definition desired is much lower than available from current anatomical imaging methods (CT or magnetic resonance).

The current utility of small-scale dosimetry essentially lies in preclinical validation of targeted radionuclide therapy. Dose modeling may be performed, to assess the relevance of a given radionuclide within a given context, or the dosimetric impact of factors such as medium heterogeneity on the dose delivery pattern. Still the potential of small-scale dosimetry clearly lies in conjunction with biological experiments both for in vitro cellular and in vivo animal studies.

References

1. Chatal JF, Hoefnagel CA: Radionuclide therapy. Lancet 354:931-935, 1999
2. Wagner HN, Wiseman GA, Marcus CS, et al: Administration guidelines for radioimmunotherapy of non-Hodgkin's lymphoma with (90)Y-labeled anti-CD20 monoclonal antibody. J Nucl Med 43:267-272, 2002
3. Jurcic JG, Larson SM, Sgouros G, et al: Targeted alpha particle immunotherapy for myelosis leukemia. Blood 100:1233-1239, 2002
4. Allen BJ, Tian Z, Rizvi S, et al: Preclinical studies of targeted alpha therapy for breast cancer using 213Bi-labelled-plasminogen activator inhibitor type 2. Br J Cancer 88:944-950, 2003
5. Allen BJ, Raja C, Rizvi S, et al: Intralesional targeted alpha therapy for metastatic melanoma. Cancer Biol Ther 4:1318-1324, 2005
6. Nilsson S, Larsen RH, Fossa SD, et al: First clinical experience with alpha-emitting radium-223 in the treatment of skeletal metastases. Clin Cancer Res 11:4451-4459, 2005
7. Rotmensch J, Schwartz JL, Atcher RW, et al: Increased nuclear damage by high linear energy transfer radioisotopes applicable for radiodirected therapy against radiologic malignancies. Gynecol Obstet Invest 32:180-184, 1991
8. Adelstein SJ, Kassis AI, Bodei L, et al: Radiotoxicity of iodine-125 and other auger-electron-emitting radionuclides: Background to therapy. Cancer Biother Radiopharm 18:301-316, 2003
9. Nikjoo H, Girard P, Charlton DE, et al: Auger electrons—a nanoprobe for structural, molecular and cellular processes. Radiat Prot Dosimetry 122:72-79, 2006
10. Loevinger R, Berman M: A Schema for Absorbed Dose Calculations or Biologically Distributed Radionuclides: MIRD Pamphlet No. 1. New York, NY, The Society of Nuclear Medicine, 1968
11. Snyder WS, Ford MR, Warner GG: "S," Absorbed Dose per Unit Calculated Activity for Selected Radionuclides and Organs: MIRD Pamphlet No. 11. New York, NY, The Society of Nuclear Medicine, 1975
12. Bouchet LG, Bolch WE, Blanco HP, et al: MIRD Pamphlet No 19: absorbed fractions and radionuclide S values for six age-dependent multiregion models of the kidney. J Nucl Med 44:1113-1147, 2003
13. Kassis AI: The MIRD approach: Remembering the limitations. J Nucl Med 33:781-782, 1992
14. Howell RW: The MIRD Schema: From organ to cellular dimensions. J Nucl Med 35:531-533, 1994
15. Kwok CS, Bialobzyski PJ, Yu SK: Effect of tissue inhomogeneity on dose distribution of continuous activity of low-energy electrons in bone marrow cavities with different topologies. Med Phys 18:533-541, 1991
16. Stabin MG, Eckerman K: Dose conversion factors for marrow and bone by skeletal regions. J Nucl Med 35:112, 1994
17. Eckerman KF, Stabin MG: Electron absorbed fractions and dose conversion factors for marrow and bone by skeletal regions. Health Phys 78:199-214, 2000
18. Fisher DR: The microdosimetry of monoclonal antibodies labeled with alpha emitters, in Schlafke-Stelson AT, Watson EE (eds): Proceedings of the Fourth International Radiopharmaceutical Dosimetry Symposium. Oak Ridge, TN, Oak Ridge Associated Universities, 1985, pp 26-36
19. Humm JL: A microdosimetric model of astatine-211 labeled antibodies for radioimmunotherapy. Int J Radiat Oncol Biol Phys 13:1767-1773, 1987
20. Stinchcomb TG, Roeske JC: Analytic microdosimetry for radioimmunotherapeutic alpha emitters. Med Phys 19:1385-1393, 1992
21. Charlton DE, Humm JL: A method of calculating initial DNA strand breakage following the decay of incorporated 125I. Int J Radiat Biol Relat Stud Phys Chem Med 53:353-365, 1988
22. Buchegger F, Perillo-Adamer F, Dupertius YM, et al: Auger radiation targeted into DNA: A therapy perspective. Eur J Nucl Med Mol Imaging 33:1352-1363, 2006
23. Nikjoo H, Martin RF, Charlton DE, et al: Modelling of Auger-induced DNA damage by incorporated 125I. Acta Oncol 35:849-856, 1996
24. Elmroth K, Stenerlöw B: Influence of chromatin structure on induction of double-strand breaks in mammalian cells irradiated with DNA-incorporated 125I. Radiat Res 168:175-182, 2007
25. Stabin MG, Siegel JA: Physical models and dose factors for use in internal dose assessment. Health Phys 85:294-310, 2003
26. Bouchet LG, Bolch WE, Weber DA, et al: MIRD Pamphlet No. 15: Radionuclide S values in a revised dosimetric model of the adult head and brain. J Nucl Med 40:62, 1999
27. Mardirossian G, Tagesson M, Blanco P, et al: A new rectal model for dosimetry applications. J Nucl Med 40:1524-1531, 1999
28. Ceccarelli C, Canale D, Battisti P, et al: Testicular function after 131I therapy for hyperthyroidism. Clin Endocrinol 65:446-452, 2006
29. Bouchet LG, Bolch WE, Howell RW, et al: S values for radionuclides localized within the skeleton. J Nucl Med 41:189-212, 2000
30. Eckerman KF, Stabin MG: Electron absorbed fractions and dose conversion factors for marrow and bone by skeletal regions. Health Phys 78:199-214, 2000
31. Coffey JL, Cristy M, Warner GG: Specific absorbed fractions for photon sources uniformly distributed in the heart chambers and heart wall of a heterogeneous phantom. J Nucl Med 22:65-71, 1981
32. McAfee JG: Problems in evaluating the radiation dose for radionuclides excreted by the kidneys, in Cloutier R, Edwards, CL, Snyder, WS (eds): Medical Radionuclides: Radiation Dose and Effects. Oak Ridge, TN, Atomic Energy Commission, 1969, pp 271-294
33. Bolch WE, Bouchet LG, Robertson JS, et al: MIRD pamphlet No. 17: The dosimetry of nonuniform activity distributions-radionuclide S values at the voxel level. J Nucl Med 40:11P, 1999 (suppl 1)
34. Zankl M, Petoussi-Henss N, Fill U, et al: The application of voxel phantoms to the internal dosimetry of radionuclides. Radiat Prot Dosimetry 105:539-548, 2003
35. Smith T P-HN, Zankl M: Comparison of internal radiation doses estimated by MIRD and voxel techniques for a "family" of phantoms. Eur J Nucl Med:1387-1398, 2000
36. Rao DV, Govelitz GF, Sastry KS: Radiotoxicity of thallium-201 in mouse testes: Inadequacy of conventional dosimetry. J Nucl Med 24: 145-153, 1983
37. Makrigiorgos GM, Ito S, Baranowska-Kortylewicz J, et al: Inhomogeneous deposition of radiopharmaceuticals at the cellular level: Experimental evidence and dosimetric implications. J Nucl Med 31:1358-1363, 1990
38. Goddu M, Howell RW, Bouchet L, et al (eds): MIRD cellular S values: Self-absorbed dose per unit cumulated activity for selected radionuclides and monoenergetic electron and alpha particle emitters incorporated into different cell compartments. Reston, VA, Society of Nuclear Medicine, 1997
39. Hindorf C, Emfietzoglou D, Linden O, et al: Internal microdosimetry for single cells in radioimmunotherapy of B-cell lymphoma. Cancer Biother Radiopharm 20:224-230, 2005
40. Champion C, Zanotti-Fregonara P, Hindie E: CELLDOSE: A Monte Carlo code to assess electron dose distribution—S values for 131I in spheres of various sizes. J Nucl Med 49:151-157, 2008
41. Bardies M, Chatal JF: Absorbed doses for internal radiotherapy from

22 beta-emitting radionuclides: Beta dosimetry of small spheres. Phys Med Biol 39:961-981, 1994
42. Li WB, Friedland W, Pomplun E, et al: Track structures and dose distributions from decays of (131)I and (125)I in and around water spheres simulating micrometastases of differentiated thyroid cancer. Radiat Res 156:419-429, 2001
43. Sgouros G: Toward patient-friendly cell-level dosimetry. J Nucl Med 48:496-497, 2007
44. Bolch WE: Alpha-particle emitters in radioimmunotherapy: New and welcome challenges to medical internal dosimetry. J Nucl Med 42: 1222-1224, 2001
45. Howell RW, Rao DV, Hou DY, et al: The question of relative biological effectiveness and quality factor for auger emitters incorporated into proliferating mammalian cells. Radiat Res 128:282-292, 1991
46. Howell RW, Wessels BW, Loevinger R, et al: The MIRD perspective 1999. J Nucl Med 40:3S-10S, 1999
47. Mausner LF, Srivastava SC: Selection of radionuclides for radioimmunotherapy. Med Phys 20:503-9, 1993
48. Wessels BW, Rogus RD: Radionuclide selection and model absorbed dose calculations for radiolabeled tumor associated antibodies. Med Phys 11:638-645, 1984
49. Weber DA, Eckerman KF, Dillman LT, et al: MIRD: Radionuclide data and decay schemes. New York, The Society of Nuclear Medicine, 1989
50. Berger MJ: MIRD Pamphlet No. 7: Distribution of absorbed doses around point sources of electrons and beta particles in water and other media. J Nucl Med 12:5-23, 1971
51. Berger MJ: Beta-ray dosimetry calculations with the use of point kernels, in Cloutier RJ, Edwards CL, Snyder WS (eds): Editors Medical radionuclides: Radiation Dose and Effects. Washington, DC, US Atomic Energy Commission, 1970, pp 63-86
52. Bardies M, Kwok C, Sgouros G: Dose point-kernels for radionuclide dosimetry, in Zaidi H, Sgouros G (eds): Therapeutic applications of Monte Carlo calculations in Nuclear Medicine. Bristol and Philadelphia, PA, IOP, 2003, pp 158-174
53. Cross WG, Williams G: Tables of Beta Dose Distributions. Chalk River, ON, Canada, Atomic Energy of Canada Limited, 1967
54. Berger MJ: Monte Carlo calculation of the penetration of diffusion of fast charged particles, in Alder B (ed): Methods in Computational Physics, New York, NY, Academic Press, 1963, pp 135-215
55. Berger MJ: Improved Point Kernels for Electrons and Beta-ray Dosimetry. Gaithersburg, MD, National Bureau of Standards, 1973
56. Prestwich WV, Nunes J, Kwok CS: Beta dose point kernels for radionuclides of potential use in radioimmunotherapy. J Nucl Med 30: 1036-1046, 1989
57. Loevinger R, Holt JG: Internally administered radioisotopes, in Hine GJ, Brownell GL (eds): Radiation Dosimetry. New York, NY, Academic Press, 1965, pp 801-873
58. Spencer LV: Theory of electron penetration. Phys Rev 98:1597-1615, 1955
59. Cross WG, Ing N, Freeman N, et al: Tables of Beta-Ray Dose Distributions in Water, Air and Other Media. Chalk River, ON, Canada, Atomic Energy of Canada Limited, 1982
60. Simpkin DJ, Mackie TR: EGS4 Monte Carlo determination of the beta dose kernel in water. Med Phys 17:179-186, 1990
61. Fujimori K, Fisher DR, Weinstein JN: Integrated microscopic-macroscopic pharmacology of monoclonal antibody radioconjugates: The radiation dose distribution. Cancer Res 51:4821-4827, 1991
62. Ferrer L, Chouin N, Bitar A, et al: Implementing dosimetry in GATE: dose-point kernel validation with GEANT4 4.8.1. Cancer Biother Radiopharm 22:125-129, 2007
63. Langmuir VK, Sutherland RM: Dosimetry models for radioimmunotherapy. Med Phys 15:867-873, 1988
64. Sastry KSR, Haydock C, Basha AM, et al: Electron dosimetry for radioimmunotherapy: Optimal electron energy. Rad Prot Dosim 13: 249-252, 1985
65. Roberson PL, Ten Haken RK, McShan DL, et al: Three-dimensional tumor dosimetry for radioimmunotherapy using serial autoradiography Int J Radiat Oncol Biol Phys 24:329-334, 1992
66. Akabani G, Hawkins WG, Eckblader MB, et al: Patient-specific dosimetry using quantitative SPECT imaging and three-dimensional discrete Fourier transform convolution. J Nucl Med 38:308-314, 1997
67. Erdi AK, Yorke ED, Loew MH, et al: Use of the fast Hartley transform for three-dimensional dose calculation in radionuclide therapy. Med Phys 25:2226-2233, 1998
68. Stabin MG, Konejnenberg M, Knapp FF, et al: Monte Carlo modeling of radiation dose distribution in intravascular radiation therapy. Med Phys 27:1086-1092, 2000
69. Hui TE, Fisher DR, Kuhn JA, et al: A mouse model for calculating cross-organ beta doses from yttrium-90-labeled immunoconjugates. Cancer 73:951-957, 1994 (suppl 3)
70. Hindorf C, Ljungberg M, Strand SE: Evaluation of parameters influencing S values in mouse dosimetry. J Nucl Med 45:1960-1965, 2004
71. Miller WH, Hartmann-Siantar C, Fisher D, et al: Evaluation of beta-absorbed fractions in a mouse model for 90Y, 188Re, 166Ho, 149Pm, 64Cu, and 177Lu radionuclides. Cancer Biother Radiopharm 20:436-449, 2005
72. Kolbert KS, Watson T, Marte C, et al: Murine S factors for liver, spleen, and kidney. J Nucl Med 44:784-791, 2003
73. Stabin MG, Peterson TE, Holburn GE, et al: Voxel-based mouse and rat models for internal dose calculations. J Nucl Med 47:655-659, 2006
74. Bitar A, Lisbona A, Thedrez P, et al: A voxel-based mouse for internal dose calculations using Monte Carlo simulations (MCNP). Phys Med Biol 52:1013-1025, 2007
75. Larsson E, Strand SE, Ljundberg M, et al: Mouse S-factors based on Monte Carlo simulations in the anatomical realistic Moby phantom for internal dosimetry. Cancer Biother Radiopharm 22:438-442, 2007
76. Briesmeister JF: MCNP—A general Monte Carlo Code for Neutron and Photon Transport. Los Alamos, NM, Los Alamos National Laboratory, 1997
77. Bitar A, Lisbona A, Bardies M: S-factor calculations for mouse models using Monte-Carlo simulations. Q J Nucl Med Mol Imaging 51:343-351, 2007
78. Cloutier RJ Watson EE: Radiation dose from isotopes in the blood, in Cloutier RJ, Edwards CL, Snyder WS (eds): Medical radionuclides: Radiation Dose and Effects. Oak Ridge, TN, US Atomic Energy Commission, 1970, pp 325-346
79. ICRP Publication 30: Limits for Intakes of Radionuclides by Workers. New York, NY, Pergamon Press, 1979
80. Bouchet LG, Bolch WE, Howell RW, et al: S values for radionuclides localized within the skeleton. J Nucl Med 41:189-212, 2000
81. Nelson WR, Hirayama H, Rogers DW: The EGS4 code system. Stanford, CA, Stanford Linear Accelerator Center, 1985
82. Stabin MG, deLuz LC: Evolution and status of bone and marrow dose models. Cancer Biother Radiopharm 17:427-433, 2002
83. Stabin MG, Sparks RB, Crowe E: OLINDA/EXM: The second-generation personal computer software for internal dose assessment in nuclear medicine. J Nucl Med 46:1023-1027, 2005
84. Zalutsky MR, Stabin MG, Larsen RH, et al: Tissue distribution and radiation dosimetry of astatine-211-labeled chimeric 81C6, an alpha-particle-emitting immunoconjugate. Nucl Med Biol 24:255–251, 1997
85. Couturier O, Faivre-Chauvet A, Filippovich IV, et al: Validation of 213Bi-alpha radioimmunotherapy for multiple myeloma. Clin Canc Res 5:3165s-3170s, 1999
86. Sgouros G, Ballangrud AM, Jurcic JG, et al: Pharmacokinetics and dosimetry of an alpha-particle emitter labeled antibody: 213Bi-HuM195 (Anti-CD33) in patients with leukemia. J Nucl Med 40: 1935-1946, 1999
87. Hall EJ: Radiobiology for the Radiologist. Philadelphia PA, Lippincott, Williams and Wilkins, 2000
88. Roeske JC, Humm JL: Microdosimetry of targeted radionuclides, in Zaidi H, Sgouros G (eds): Therapeutic Applications of Monte Carlo Calculations in Nuclear Medicine. Bristol, Institute of Physics Publishing, 2003, pp 202-227
89. Polig E: The localized dosimetry of internally deposited alpha-emitters. Curr Top Radiat Res 13:189-327, 1978

90. Rossi HH: Microdosimetric energy distribution in irradiated matter, in Attix FH, Roesch WC (eds): Radiation Dosimetry Vol. I. Fundamentals. New York, NY, Academic Press, 1968, pp 43-92
91. Roesch WC: Microdosimetry of internal sources. Radiat Res 70:494-510, 1977
92. Booz J, Coppola M: Energy deposition by fast neutrons to small spheres, in Booz J, Ebert HG, Eickel R, et al (eds): Proceedings of the Fourth Symposium on Microdosimetry. Verbana Pallanza, Italy, 1974, EUR 5112 d-e-f 983-1000:983-1000
93. Wilson WE, Paretzke HG: Calculation of ionization frequency distributions in small sites. Radiat Res 81:326-335, 1980
94. Berger MJ: Methods in computational physics, in Booz J, Ebert HG, Eickel R, et al (eds): Proceedings of the Fourth Symposium on Microdosimetry. Verbana Pallanza, Italy, 1974, EUR 5112 d-e-f 983-1000: 695-715
95. Kellerer AM: Analysis of patterns of energy deposition: A survey of theoretical relations in microdosimetry, in Ebert HG (ed): Proceedings of the Second Symposium on Microdosimetry. Brussels, 1970, EUR 4452 d-e-f 107-34
96. Incerti S, Gault N, Habchi C, et al: A comparison of cellular irradiation techniques with alpha particles using the Geant4 Monte Carlo simulation toolkit. Radiat Prot Dosimetry 122:327-329, 2006
97. Roeske JC, Hoggarth M: Alpha-particle Monte Carlo simulation for microdosimetric calculations using a commercial spreadsheet. Phys Med Biol 52:1909-1922, 2007
98. Eckerman KF, Ryman JC, Taner AC, et al: Traversal of cells by radiation and absorbed dose fraction estimates for electrons and alpha particles, in Schlafke-Stelson AT, Watson EE (eds): Proceedings of the Fourth International Radiopharmaceutical Dosimetry Symposium. Oak Ridge, TN, Oak Ridge Associated Universities, 1985, pp 67-81
99. Bichsel H: Stopping Powers of Fast Charged Particles in Heavy Elements. NIST Report IR-4550. Springfield, VA, US National Technical Information Service, 1992
100. ICRU: Stopping powers and ranges for protons and alpha particles, Report No. 49, Bethesda, MD, International Commission of Radiation Units, 1993
101. Ziegler JF: The stopping of energetic light ions in matter. Appl Phys Rev 85:1249-1272, 1999
102. Attix FH: Introduction to Radiological Physics and Radiation Dosimetry. New York, NY, John Wiley and Sons, 1986
103. Janni JF: Calculation of energy loss, range, path length, straggling, multiple scattering and the probability of inelastic nuclear collisions for 0.1 to 1000 MeV protons Technical Report No. AFWL-TR-65-150. Washington, DC, 1966
104. Walsh PJ: Stopping power and range of alpha particles. Health Phys 19:312-316, 1970
105. Stinchcomb TG, Roeske JC: Values of "S", <z1> and <z12> for dosimetry using alpha-particle emitters. Med Phys 26:1960-1971, 1999
106. Charlton DE, Sephton R: A relationship between microdosimetric spectra and cell survival for high-LET irradiation. Int J Radiat Biol 59:447-457, 1991
107. Humm JL, Chin LM: A model of cell inactivation by alpha-particle internal emitters. Radiat Res 134:143-150, 1993
108. Stinchcomb TG, Roeske JC: Survival of alpha particle irradiated cells as a function of the shape and size of the sensitive target (nucleus). Radiat Prot Dosim 62:157-164, 1995
109. Kvinnsland Y, Stokke T, Aurilien E: Radioimmunotherapy with alpha-particle emitters: Microdosimetry of cells with heterogeneous antigen expression and with various diameters of cells and nuclei. Radiat Res 155:288-296, 2001
110. Charlton DE: The survival of monolayers of cells growing in clusters irradiated by 211At appended to the cell surfaces. Radiat Res 151: 750-753, 1999
111. Aurlien E, Larsen RH, Akabani G, et al: Exposure of human osteosarcoma and bone marrow cells to tumor-targeted alpha-particles and gamma-irradiation: Analysis of cell survival and microdosimetry. Int J Radiat Biol 76:1129-1141, 2000
112. Larsen RH, Akabani G, Welsh P: The cytotoxicity and microdosimetry of astatine-211-labeled chimeric monoclonal antibodies in human glioma and melanoma cells in vitro. Radiat Res 149:155-162, 1998
113. Stinchcomb TG, Roeske JC: Analysis of survival of C-18 cells after irradiation in suspension with chelated and ionic bismuth-212 using microdosimetry. Radiat Res 140:48-54, 1994
114. Kennel SJ, Stabin M, Roeske JC, et al: Radiotoxicity of bismuth-231 bound to membranes of monolayer and spheroid cultures of tumor cells. Radiat Res 151:244-256, 1999
115. Charlton DE: Radiation effects in spheroids of cells exposed to alpha emitters. Int J Radiat Biol 76:1555-1564, 2000
116. Smilenov LB, Hall EJ, Bonner WM, et al: A microbeam study of DNA double-strand breaks in bystander primary human fibroblasts. Radiat Prot Dosim 122:256-259, 2006
117. Humphreys ER, Humm JL: A Monte-Carlo approach to the microdosimetry of 224Ra in murine compact and cancellous bone. Health Phys 54:607-615, 1988
118. Charlton DE, Utteridge TD, Beddoe AH: Microdosimetry of haemopoietic stem cells irradiated by alpha particles from short-lived products of 222Rn decays in fat cells and heamopoietic tissue. Int J Radiat Biol 69:585-592, 1996
119. Charlton DE, Salmon PL, Utteridge TD: Monte Carlo/numerical treatment of alpha-particle spectra from sources buried in bone and resultant doses to surface cells. Int J Radiat Biol 73:89-92, 1998
120. Austin AL, Ellender M, Haines JW, et al: Microdistribution and localized dosimetry of the alpha-emitting radionuclides 239 Pu, 241Am and 233U in mouse femoral shaft. Int J Radiat Biol 76:101-111, 2000
121. Akabani G, Zalutsky MR: Microdosimetry of astatine-211 using histological images: Application to bone marrow. Radiat Res 148:599-607, 1997
122. Rajon DA, Jokisch DW, Patton PW, et al: Voxel effects within digital images of trabecular bone and their consequences on chord-length distributions measurements. Phys Med Biol 47:1741-1759, 2002
123. Hunt JG, Watchman CJ, Bolch WE: Calculation of absorbed fractions to human skeletal tissues due to alpha particles using monte carlo and 3-D chord-based transport techniques. Radiat Prot Dosim, 2007
124. Utteridge TD, Charlton DE, Allen BJ: Monte Carlo modeling of the effects of injected short-, medium- and longer-range alpha-particle emitters on human marrow at various ages. Radiat Res 156:413-418, 2001
125. Fakir H, Hofmann W: Incorporation of microdosimetric concepts into a biologically-based model of radiation carcinogenesis. Radiat Prot Dosim 122:330-334, 2006.
126. Charlton DE, Booz J: A Monte Carlo treatment of the decay of 125I. Radiat Res 87:10-23, 1981
127. Chung MF, Jenkins LH: Auger electron energies of the outer shell electrons. Surf Sci 22:479-485, 1970
128. Pomplun E, Booz K, Charlton DE: A Monte Carlo simulation of Auger electron cascades. Rad Res 111:553–552, 1987
129. Desclaux JP: A multi-configuration relativistic Dirac-Fock program. Comput Phys Commun 9:31-45, 1976
130. Carlson TA, White RM: Formation of fragment ions from CH3125Te and C2H5125Te following the nuclear decay of CH3125I and C2H5125I. J Chem Phys 38:2930-2934, 1964
131. Ertl HH, Feinendegen LE, Heiniger HJ: Iodine-125, a tracer in cell biology: Physical properties and biological aspects. Phys Med Biol 15:447-456, 1970
132. Burki HJ, Roots R, Feinendegen LE, et al: Inactivation of mammalian cells after disintegration of 3H or 125I in cell DNA at −196 degrees C. Int J Radiat Biol Relat Stud Phys Chem Med 24:363-375, 1973
133. Hofer KG, Keough G, Smith JM: Biological toxicity of Auger emitters: Molecular fragmentation versus electron irradiation. Curr Top Radiat Res Q 12:335-354, 1978
134. Yasui LS, Hofer KG: Role of mitochondrial DNA in 125I decay induced cell death. Int J Radiat Biol 49:601-610, 1986
135. Hofer KG: Biophysical aspects of Auger processes—A review. Acta Oncol 35:789-796, 1996
136. Kassis AI, Fayad F, Kinsey BM, et al: Radiotoxicity of an 125I labeled DNA intercalator in Mammalian Cells. Radiat Res 118:283-294, 1989
137. Sastry KS: Biological effects of the Auger emitter iodine-125: A review.

Report No. 1 of AAPM Nuclear Medicine Task Group No. 6. Med Phys 19:1361-1370, 1992
138. Kassis AI, Adelstein SJ, Haydock C, et al: Lethality of Auger electrons from the decay of bromine-77 in the DNA of mammalian cells. Radiat Res 90:362-373, 1982
139. Makrigiorgos GM, Berman RM, Baranowska-Kortylewicz J, et al: DNA damage produced in V79 cells by DNA-incorporated iodine-123: A comparison with iodine-125. Radiat Res 129:309-314, 1992
140. Kassis AI, Adelstein SJ, Haydock C, et al: Thallium-201: An experimental and a theoretical radiobiological approach to dosimetry. J Nucl Med 24:1164-1175, 1983
141. Rao DV, Shepstone BJ, Wilkins HB, et al: Kinetics and dosimetry of thallium-201 in human testes. J Nucl Med 36:607-609, 1995
142. Pomplun E, Terrissol M, Kümmerle E: Estimation of a radiation weighting factor for 99mTc. Radiat Prot Dosim 122:80-81, 2006
143. Narra VR, Sastry KS, Goddu SM, et al: Relative biological effectiveness of 99mTc radiopharmaceuticals. Med Phys 21:1921-1926, 1994
144. Howell RW: Radiation spectra for Auger-electron emitting radionuclides: Report No. 2 of AAPM Nuclear Medicine Task Group No. 6. Med Phys 19:1371-1383, 1992
145. Humm JL, Howell RW, Rao DV: Dosimetry of Auger-electron-emitting radionuclides: Report no. 3 of AAPM Nuclear Medicine Task Group No. 6. Med Phys 21:1901-1915, 1994
146. Humm JL, Charlton DE: A new calculational method to assess the therapeutic potential of Auger electron emission. Int J Radiat Oncol Biol Phys 17:351-360, 1989
147. Martin RF, Haseltine WA: Range of radiochemical damage to DNA with decay of iodine-125. Science 213:896-898, 1981
148. Terrissol M, Pomplun E: A nucleosome model for the simulation of DNA strand break experiments. Basic Life Sci 63:243-250, 1994
149. Terrissol M, Edel S, Pomplun E: Computer evaluation of direct and indirect damage induced by free and DNA-bound iodine-125 in the chromatin fibre. Int J Radiat Biol 80:905-908, 2004
150. ICRU Report 67: Absorbed-Dose Specification in Nuclear Medicine. Ashford, UK, International Commission of Radiation Units, Nuclear Technology Publishing, 2002
151. Goddu SM, Howell RW, Rao DV: Calculation of equivalent dose for Auger electron emitting radionuclides distributed in human organs. Acta Oncol 35:909-916, 1996
152. Liber HL, LeMotte PK, Little JB: Toxicity and mutagenicity of X-rays and [125I]dUrd or [3H]TdR incorporated in the DNA of human lymphoblast cells. Mutat Res 111:387-404, 1983